ACS APPLIED MATERIALS & INTERFACES

Research Article

www.acsami.org

Nanoporous Gold as a Neural Interface Coating: Effects of Topography, Surface Chemistry, and Feature Size

Christopher A. R. Chapman,[†] Hao Chen,[‡] Marianna Stamou,[‡] Juergen Biener,[§] Monika M. Biener,[§] Pamela J. Lein,[‡] and Erkin Seker*[,∥]

[†]Department of Biomedical Engineering, [‡]Department of Molecular Biosciences, and [∥]Department of Electrical and Computer Engineering, University of California—Davis, Davis, California 95616, United States

[§]Lawrence Livermore National Laboratory, Livermore, California 94551, United States

Supporting Information

ABSTRACT: Designing neural interfaces that maintain close physical coupling of neurons to an electrode surface remains a major challenge for both implantable and in vitro neural recording electrode arrays. Typically, low-impedance nanostructured electrode coatings rely on chemical cues from pharmaceuticals or surface-immobilized peptides to suppress glial scar tissue formation over the electrode surface (astrogliosis), which is an obstacle to reliable neuron−electrode coupling. Nanoporous gold (np-Au), produced by an alloy corrosion process, is a promising candidate to reduce astrogliosis solely through topography by taking advantage of its tunable length scale. In the present in vitro study on np-Au's interaction with cortical neuron−glia co-cultures, we demonstrate that the nanostructure of np-Au achieves close physical coupling of neurons by maintaining a high neuron-to-astrocyte surface coverage ratio. Atomic layer deposition-based surface modification was employed to decouple the effect of morphology from surface chemistry. Additionally, length scale effects were systematically studied by controlling the characteristic feature size of np-Au through variations in the dealloying conditions. Our results show that np-Au nanotopography, not surface chemistry, reduces astrocyte surface coverage while maintaining high neuronal coverage and may enhance neuron−electrode coupling through nanostructure-mediated suppression of scar tissue formation.

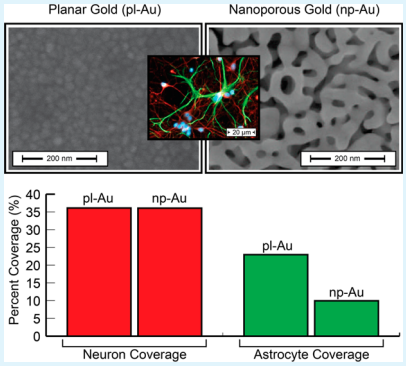

KEYWORDS: *neural electrode, nanostructure, cell−material interaction, nanoporous gold, neuron−astrocyte co-culture, nanotopography, multifunctional biomaterial, gliosis*

1. INTRODUCTION

Neural interfaces (e.g., implantable electrodes and planar multiple-electrode arrays) have emerged in the past few decades as transformative tools to monitor and modulate neural electrophysiology for fundamental studies of the nervous system, as well as to diagnose and treat neurological disorders.[1] These interfaces require low electrical impedance to reduce background noise and close physical coupling between the electrode and neurons for enhanced recording fidelity. An important obstacle in maintaining robust physical neuron−electrode coupling both in vitro and in vivo is the encapsulation of the electrode by reactive glia (astrogliosis, an important contributor to scar tissue), leading to neuronal death or detachment in the vicinity of the electrode.[2−5] To that end, substantial efforts have been devoted to engineering multifunctional electrode coatings that can both maintain low electrical impedance and mitigate astrogliosis to promote strong neuron−electrode coupling.[6] Nanostructured materials[7−13] have shown promise as multifunctional coatings for neural interfaces, maintaining low impedance through a large effective surface area and mitigating astrogliosis through chemical cues, such as local administration of pharmacological agents[14] and surface display of immobilized peptides.[15] Very few studies have investigated the effect of topographical cues in controlling astrogliosis due in part to the complexity of studying both glia and neurons on varying surface morphologies. Ultimately, nanostructured materials for use in neural interfaces need the ability to use both chemical and topographical cues to achieve the desired tissue response. Nanoporous gold (np-Au), a nanostructured material typically produced by dealloying of gold−silver alloys,[16] that is, by selective dissolution of the silver component in nitric acid, enables both chemical and topographical cues to be employed to control neural tissue response. The np-Au film is composed of a network of gold ligaments and pores tens of nanometers in size (Figure 1a) with both pores and ligaments acting as nanoscale topographical cues. Np-Au has already attracted significant interest for its use in electrochemical sensors,[17−21] catalytic platforms,[17,22] fundamental structure−property studies at the nano scale,[21,23,24] and tunable drug release.[25] It combines many other attractive features as well, such as high effective surface area,[17] tunable pore size,[26] well-defined conjugate chemistry,[27] high electrical

Received: January 14, 2015
Accepted: February 23, 2015
Published: February 23, 2015

DOI: 10.1021/acsami.5b00410
ACS Appl. Mater. Interfaces 2015, 7, 7093−7100

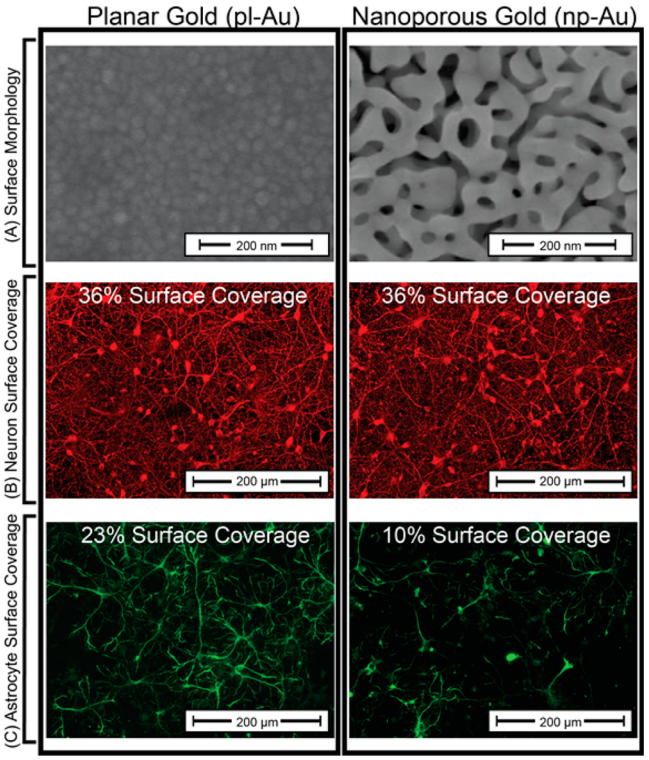

Figure 1. (A) Scanning electron micrographs of pl-Au and np-Au show marked differences in surface morphology. (B) Fluorescent images of β-tubulin immunopositive cells (red) show high neuron coverage on both pl-Au and np-Au. (C) Fluorescent images of GFAP immunopositive cells (green) indicate astrocyte coverage on np-Au that is significantly reduced compared to pl-Au. Numerical values of the cell surface coverage are provided for quantitative comparison of the fluorescent images.

conductivity, and compatibility with traditional fabrication techniques.[28] The suitability of np-Au as a multifunctional neural electrode coating is highlighted in recent studies that demonstrate its application in high-fidelity recordings from organotypic brain slices,[29] biocompatibility,[29−31] in situ drug delivery for reducing astrocytic proliferation,[31] on demand drug release,[18,32] and biofouling-resistant electrical performance.[33] Here, we report the novel ability of np-Au to reduce astrocytic coverage through topographical cues. The length scale of the np-Au structure and its surface chemistry were independently controlled by altering the dealloying conditions as well as atomic layer deposition (ALD)-based surface functionalization, respectively. This allowed us to differentiate between topographical and surface chemical effects. A primary neuron−glia co-culture model, derived from the perinatal rat neocortex, is used to accurately simulate the neural tissue environment in vitro.[34] We demonstrate that np-Au surface coatings dramatically reduce astrocytic surface coverage while maintaining normal neuronal coverage, and show that the reduction in astrocytic coverage on the np-Au surface is in fact a function of topographical cues from the nanoscale topography and is not surface chemistry mediated.

2. EXPERIMENTAL SECTION

2.1. Sample Fabrication and Characterization. Samples were typically deposited in 5 mm diameter spots onto the middle of a piranha-cleaned 12 mm diameter thin (0.15 mm thick) glass slide. Unstructured planar gold (pl-Au) samples were deposited by direct current sputtering (Kurt J. Lesker) of a 200 nm thick gold layer (at 10 mTorr Ar) on top of the substrate coated with a 160 nm thick chromium adhesion layer. Gold−silver alloy spots (precursor to np-Au) were fabricated by sputtering a 160 nm thick chromium adhesion layer, 80 nm thick gold corrosion barrier layer, and a 600 nm thick gold and silver alloy (64% silver and 36% gold; atomic (at.) %). The final np-Au films were fabricated by immersing the gold−silver alloy in heated (55 °C) nitric acid (70%) for 15 min. The short dealloying times used in the present study typically result in residual silver levels on the order of 3−5%.[25,29] Although not necessary for this study, post-treatment of the np-Au films could reduce silver levels to <1 at. %.[35] The samples were then soaked in deionized (DI) water for 1 week with the water changed every 24 h. To produce both a high silver content np-Au film with similar feature sizes and np-Au films with increased feature sizes, the nitric acid concentration was decreased to 50% with dealloying times ranging from 10 min to 24 h. ***Caution:*** *Nitric acid is highly corrosive and reactive with organic materials and must be handled with extreme care.* The morphology of the coatings was characterized by scanning electron microscopy (FEI Nova NanoSEM430), and elemental compositions before and after dealloying were assessed with energy dispersive X-ray spectroscopy (Oxford INCA, Energy-EDS). Average ligament width and pore diameter were analyzed using a custom MATLAB script by both vertical and horizontal averaging over each SEM image taken.

2.2. Cell Culture and Imaging. Primary rat cortical cells were obtained from the laboratory of Prof. Pamela J. Lein at the University of California—Davis. All studies were conducted according to protocols approved by the Institutional Animal Care and Use Committee of the University of California—Davis. Material samples were incubated with 0.5 mg/mL poly-L-lysine in B Buffer (boric acid and borax, Sigma, Saint Louis, MO) at 37 °C in 5% CO_2 for 4 h. Materials were then washed with sterile deionized (DI) water and then incubated for 12 h at 37 °C and 5% CO_2 with plating media consisting of 2% B27 supplement, 1× Glutamax, 10% heat-inactivated horse serum, and 1 M HEPES at pH 7.5 with Neurobasal A as the basal medium (all media components were obtained from Invitrogen, Carlsbad, CA). Dissociated cortical cells were plated at a density of 50,000 cells/cm^2 on each material and kept in plating medium for 4 h before being switched to a serum-free growth medium. Unless otherwise noted, cells were cultured for 7 days to allow sufficient time for the growth and coverage of neurons and astrocytes over the material surface.[3] For cellular quantification, the cells were fixed using 4% paraformaldehyde in phosphate buffered saline (Affymetrix) and immunostained using mouse anti-tubulin-βIII antibodies (Invitrogen) to visualize neurons and rabbit anti-glial fibrillary acidic protein antibodies (GFAP, Invitrogen) to visualize astrocytes, followed by incubation with goat anti-mouse antibodies conjugated to Alexa Fluor 555 (Invitrogen) and goat anti-rabbit antibodies conjugated to Alexa Fluor 488 (Invitrogen). Counterstaining with DAPI was used to visualize cell nuclei. Images of immunostained samples were acquired using an inverted fluorescence microscope (Zeiss Observer D1). Epifluorescent images were analyzed using a custom ImageJ macro[28] to determine cell coverage of a given surface.

2.3. Modification of Surface Chemistry. Some np-Au samples were coated with 2.5 nm thick Al_2O_3 films as described previously.[36] The coatings were created through the well-established trimethylaluminum ($AlMe_3/H_2O$) ALD process[37] in a warm wall reactor.

2.4. Statistical Methods. Each study was performed on at least three different samples per dissection and imaged at the same five locations on each sample. Unless otherwise stated, the reported values represent averages plus standard deviations of the measurements. A two-tailed Student's *t*-test assuming unequal variance was used to identify differences between two different sample groups. Unless otherwise noted, a one-way ANOVA was used when comparing more than two groups in each experiment. Statistical significance was determined by p-values < 0.05.

DOI: 10.1021/acsami.5b00410
ACS Appl. Mater. Interfaces 2015, 7, 7093−7100

3. RESULTS AND DISCUSSION

The np-Au films used in this study were characterized to have an average ligament width of 30.6 ± 1.2 nm and average pore diameter of 87.11 ± 4.55 (Figure 1A). These feature sizes are within a range that has been shown previously to elicit cellular responses, such as decreased cell adhesion and surface coverage.[13] We thus began this study by investigating the overall effect of np-Au on both neurons and astrocytes in co-culture through quantification of cell surface coverage in comparison to unstructured planar gold.

3.1. Effect of Au Surface Topography. To determine the cellular response to np-Au, the surface coverages (in percent of surface area covered) of both neurons and astrocytes on pl-Au and np-Au coatings were determined from digitally processed epifluorescent images (Figure 1). The neuronal surface coverage remained constant at 36% ($p > 0.9$) on both pl-Au and np-Au. However, astrocyte coverage on the np-Au surface decreased significantly ($p < 0.001$) with a 56.5% reduction in coverage from an observed 23% surface coverage on the pl-Au surface to 10% on the np-Au surface. This result demonstrates that np-Au dramatically reduces astrocytic coverage over the sample surface in a cell-type selective manner (i.e., only astrocytes are affected). This observation can be extended to suggest that reduced astrocyte coverage may allow for unobstructed neuron surface coupling on np-Au biomedical device coatings.

Although these results suggest a topographical effect, surface chemistry effects, such as residual silver in the np-Au film (either ionized into the culture medium or presented on the ligament surface), need to be ruled out as contributing factors.

3.2. Effect of Residual Silver. Potential cytotoxic effects of residual silver (ionized or surface-bound) were investigated by studying the effect of the residual silver content of np-Au films on both neuron and astrocyte surface coverage in neuron−glia co-cultures. For this, we prepared high-silver content np-Au films (HS np-Au) with approximately three times the residual silver content (~12 at. % instead of ~4 at. % silver). This film showed similar ligament width and pore diameter distributions as the standard np-Au film (34 ± 1 and 80.78 ± 3.2 nm, respectively) such that any differences in cell coverage could be attributed to the effect of residual silver (Figure 2).

Primary cortical neuron−glia co-cultures were grown on both standard np-Au and HS np-Au films and on unstructured 64% silver precursor alloy and 0% silver unstructured pl-Au.

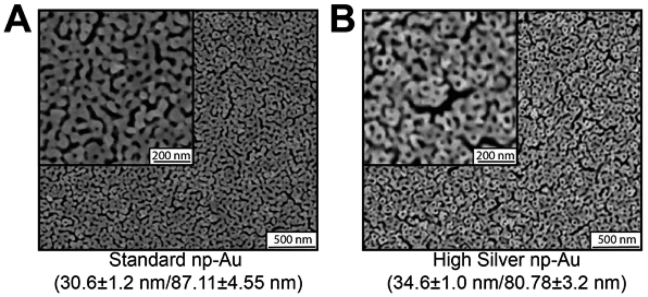

Figure 2. (A) Scanning electron micrographs of the standard (4 at. % silver) and (B) high-silver content (12 at. % silver) np-Au surfaces. The low-magnification SEM micrographs demonstrate the long-range uniformity of the np-Au substrates. (insets) High magnification (100 kX) micrographs. Measured ligament lengths and pore diameters are shown.

Comparison of fluorescence microscopy images from cultures grown on the unstructured 64% silver precursor alloy and 0% pl-Au at 7 days in vitro demonstrate a clear cytotoxic effect of silver on both neurons and astrocytes in the co-culture (Figure 3A i vs ii). HS np-Au films elicited cytotoxic reactions from

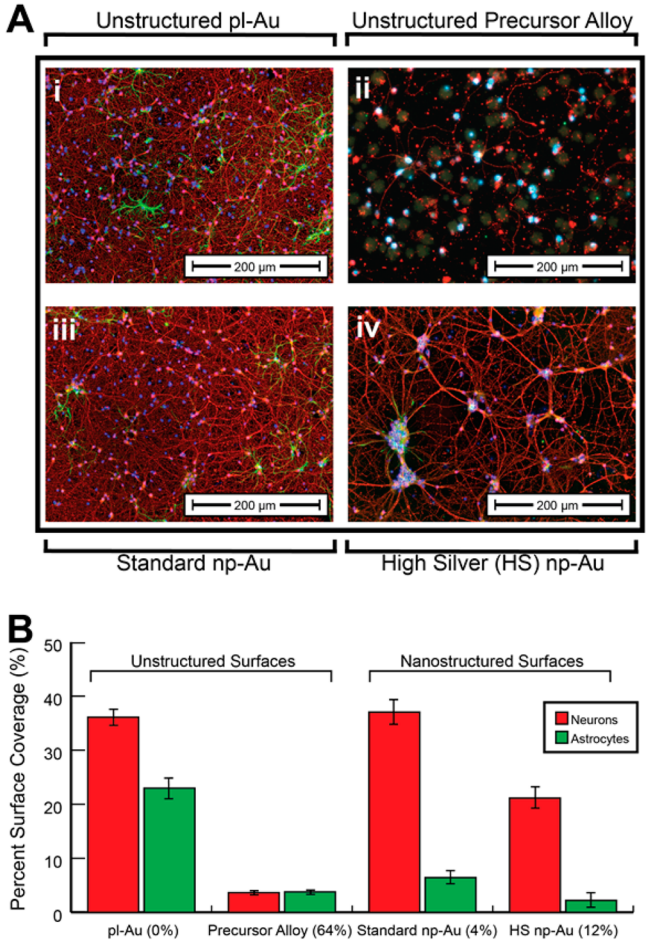

Figure 3. (A) Merged epifluorescent images of primary cortical neuron−glia co-cultures immunostained for β-tubulin (red, neurons) and GFAP (green, astrocytes) grown on unstructured pl-Au (i), unstructured precursor gold−silver alloy with 64% silver (ii), standard np-Au containing ~4 at. % silver (iii), and a high silver content np-Au film containing ~12 at. % silver (iv). (B) Surface coverage analysis of in vitro day 7 neurons and astrocytes grown on np-Au films containing varying amounts of silver (4 and 12 at. %), as well as pl-Au and the gold−silver alloy, reveals acute toxicity of the high silver np-Au with no visually observed toxicity of the standard np-Au.

both neurons and astrocytes with significant neuronal and astrocytic cell death occurring in cultures grown on the HS np-Au samples and were characterized by cellular morphologies consistent with apoptosis, such as nuclear fragmentation and neurite fasciculation (Figure 3A iv).[38−40] Although no abnormal cellular morphologies were present at the silver amounts present in the standard np-Au films, reduced astrocytic coverage was still observed (Figure 3A iii).

Although the standard np-Au film is not affecting the viability of neurons visually, these results do not rule out cytotoxic effects at the low silver levels seen in the standard np-Au film. There are two possible explanations as to why astrocytes may be more sensitive to the amount of silver on the surface than neurons: (1) astrocytes are known to sequester excess metal

DOI: 10.1021/acsami.5b00410
ACS Appl. Mater. Interfaces 2015, 7, 7093−7100

ions, such as Pb and Hg,[41,42] a phenomenon thought to protect neurons; and (2) a recent study has demonstrated that silver nanoparticles in an astrocytic cell line are more susceptible to inhibiting proliferation than in a neuronal cell line.[43]

3.3. Altering np-Au Surface Chemistry Through ALD Alumina Coating. To further rule out potential effects from the lower amounts of residual silver typically present in the standard np-Au films, we coated standard np-Au films with conformal, 2.5 nm thick aluminum oxide (Al_2O_3) ALD films. Aluminum oxide was chosen for its biocompatibility, which has been demonstrated both in vitro[44] and in vivo.[45] The conformal coating created by ALD uniformly masks the metal surface with alumina, thereby effectively masking contained silver from any potential interaction with the cells without altering the np-Au morphology (Figure 4).[36]

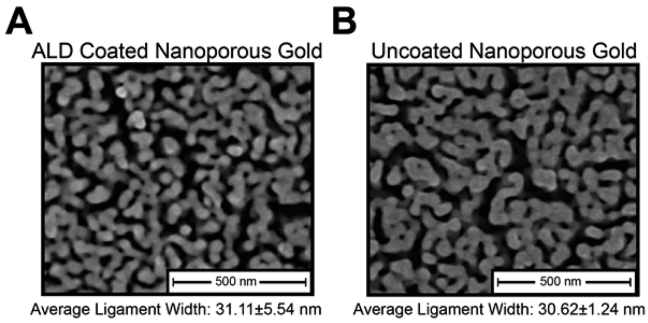

Figure 4. Scanning electron micrographs of (A) aluminum oxide-coated nanoporous gold via atomic layer deposition (ALD) and (B) uncoated nanoporous gold.

Thus, the neuron−glia co-culture experiences the same nanotopography for both samples and eliminates any interaction with residual silver in the case of the ALD-coated np-Au sample. A comparison of the neuron−glia co-cultures grown on the ALD np-Au and np-Au surfaces show similar neuron (36%) and astrocyte (10−12%) coverages (Figure 5A). This indicates that the residual silver of the standard np-Au films (i.e., 4 at. % residual silver or less) is not the primary cause of the observed reduction in astrocytic surface coverage. To further validate this finding, we also tested pl-Au and aluminum oxide-coated pl-Au (ALD pl-Au) to contrast the effects of nanostructure on cortical neuron and astrocyte surface coverage. Throughout all of the samples, the neuronal surface coverage remained constant between 35 and 37% (one-way ANOVA, $p > 0.3$). Significantly reduced astrocyte surface coverage was seen on both np-Au and ALD np-Au ($p < 0.01$). Additionally, investigating astrocyte surface coverage as a function of surface chemistry alone (i.e., aluminum oxide coating) showed no significant changes between alumina and non-alumina-coated pl-Au ($p > 0.5$) samples (Figure 5B).

This decoupling of the chemical cues from silver and np-Au nanotopography suggests that the reduction in astrocytic surface coverage seen on np-Au is primarily due to effects from the np-Au surface nanotopography (i.e., pores and ligaments) and not toxicity caused by residual silver.

3.4. Mechanism of Decreased Astrocytic Surface Coverage. The observed decrease in the area of astrocyte surface coverage can be caused by a decrease in either the number of astrocytes present on the np-Au surface (astrocyte density) or of solely the astrocyte cell area (surface coverage). A reduction in the astrocyte number (astrocyte density) on the

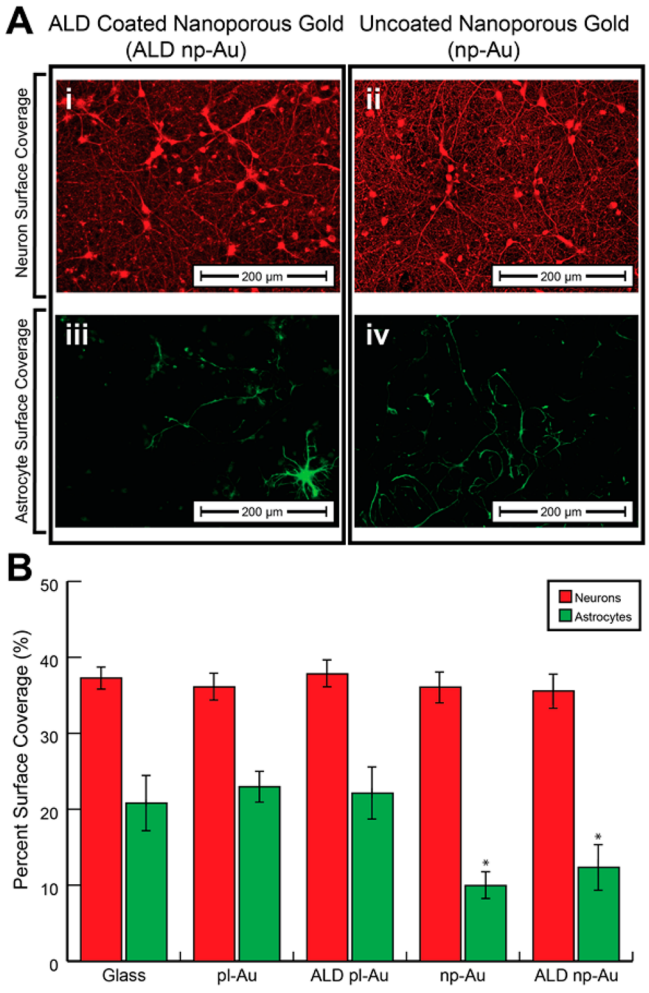

Figure 5. (A) Epifluorescent images of neuronal and astrocytic coverage on alumina-coated (i and iii) and uncoated np-Au samples (ii and iv). (B) Analysis of neuron and astrocyte surface coverage on aluminum oxide-coated np-Au and pl-Au along with uncoated np-Au and pl-Au reveal that np-Au surface morphology, and not residual silver, is the dominant mechanism through which astrocyte coverage is reduced by 48−57% in comparison to pl-Au and glass. *$p < 0.001$ in comparison to pl-Au.

surface of the material could indicate that this observed topographical response is cytotoxic, which is an undesirable method of reducing astrocytic surface coverage. To determine if the observed effect is decreasing astrocyte surface coverage through a reduction in astrocyte density or by solely reducing astrocyte cell area, co-cultures were grown on standard np-Au, pl-Au, and glass for 1, 7, and 12 days in vitro. Astrocyte cell density (number of cells per square millimeter) was quantified across substrates. As seen in Figure 6, astrocyte cell density does not decrease over time on the np-Au substrate when compared to either pl-Au or glass.

Additionally, the average proliferation rates (increase in cell density per day) were also similar for each substrate over the 12-day period (Table 1).

This finding validates that the decrease of astrocytic surface coverage seen on the standard np-Au film is not due to a reduction in astrocyte cell density or proliferation rate (i.e., cell death) and suggests that astrocytes remain viable independent of surface coverage on the np-Au surface. This is an important result that further demonstrates the potential biocompatibility

DOI: 10.1021/acsami.5b00410
ACS Appl. Mater. Interfaces 2015, 7, 7093−7100

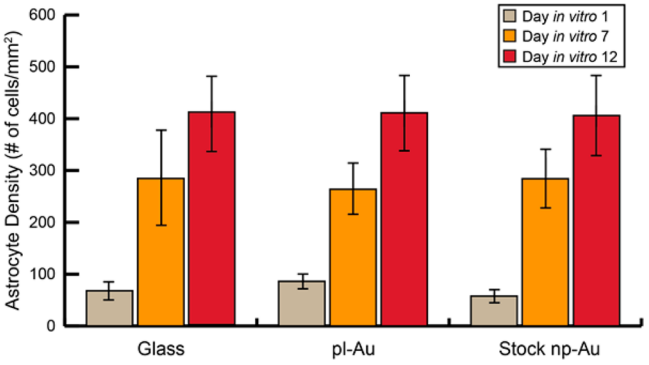

Figure 6. Quantification of astrocyte density (cells/mm^2) on glass, pl-Au, and standard np-Au surfaces at in vitro days 1, 7, and 12 showing no significant changes in astrocyte density on standard np-Au relative to either pl-Au or glass substrates.

Table 1. Proliferation Rates[a] of Astrocytes on Different Substrates

substrate	days 1−7	days 7−12	days 1−12
glass	36.11	25.04	30.57
pl-Au	29.60	29.48	29.54
standard np-Au	37.74	24.33	31.04

[a]Rate = number of cells mm^{-2} day^{-1}.

of np-Au over a time period in which the most acute cytotoxicity is expected.

3.5. Feature Size-Dependent Effects. To determine if the topographic effects of np-Au substrates on astrocytic coverage depend on the feature size of the pores and ligaments of np-Au, we fabricated a series of np-Au films with different ligament sizes (Figure 7 and Table 2) ranging from 30.6 ± 1.24 nm for standard np-Au (15 min, M1) to 88.61 ± 4.89 nm (24 h, M4). The corresponding pore diameters fell into two distinct regimes of ∼87−88 nm for M1 and M2 and ∼149 nm for M3 and M4.

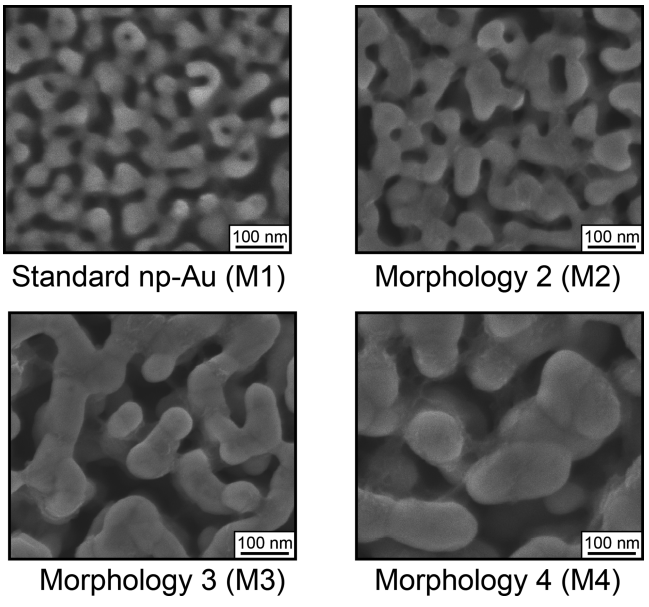

Figure 7. Scanning electron micrographs of four different np-Au surface morphologies (M1−M4) prepared by dealloying for 15 min to 24 h.

Table 2. Average Ligament Widths and Pore Diameters of Fabricated np-Au Films

film	ligament width (nm)[a]	pore diameter (nm)[a]	dealloying time
morphology 1 (M1)	30.62 ± 1.24	87.11 ± 4.55	15 min
morphology 2 (M2)	44.54 ± 1.01	88.64 ± 5.26	20 min
morphology 3 (M3)	70.65 ± 2.71	149.20 ± 11.3	40 min
morphology 4 (M4)	88.61 ± 4.89	149.24 ± 9.9	24 h

[a]Values after " ± " indicate standard error of nanofeature sizes.

Cortical neuron−glia co-cultures were then grown on each morphology for 7 days to assess feature size-dependent coverage of both neurons and astrocytes. Surface coverage analysis of both neurons and astrocytes showed a similar response to all feature sizes investigated (Figure 8). Although

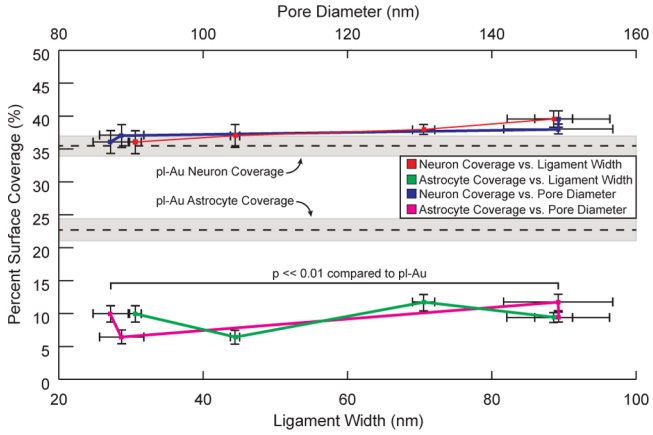

Figure 8. Quantification of neuron and astrocyte coverage vs ligament width and pore diameter on the different np-Au surface morphologies shows a similar value for neuron coverage when compared to planar gold and sustained decrease in astrocyte coverage on each morphology tested. The dashed horizontal lines and shaded regions indicate mean cell coverage and its standard deviation on pl-Au, respectively.

neuronal coverage increased slightly with increasing pore and ligament size, astrocytic coverage displayed a weak non-monotonous dependence on both pore and ligament size. However, although the neuronal coverage is similar on all np-Au morphologies and pl-Au, the astrocyte coverage on np-Au remains lower than that on pl-Au, independent of the characteristic feature size of the np-Au substrate. These results shed new light on our previous work demonstrating enhanced electrophysiological recording performance (i.e., reduced background noise and better resolved spikes) of np-Au multiple electrode arrays.[29] Reduced background noise was likely a result of reduced electrical impedance[46] stemming from the increased effective surface area of the nanoporous network; however, the 5-fold enhancement in signal strength might be due to the maintenance of strong neuron−electrode coupling by reducing the ionically insulating astrocytic coverage[2,47] on the np-Au electrode surface.

For the range of feature sizes tested, there is no significant effect of the feature size of np-Au on the surface coverage of astrocytes or neurons. In contrast to studies that employed symmetric and uniform nanotopographical features (ordered

DOI: 10.1021/acsami.5b00410
ACS Appl. Mater. Interfaces 2015, 7, 7093−7100

pillars, pits, or gratings),[48] the np-Au surface displays a repeatable distribution of features of varying size and shape. As shown in Table S1 in the Supporting Information, even though coarsening increases the average feature (i.e., ligament and pore) size, there is an overlap of feature sizes between the distributions. Therefore, the net response of a population of cells grown on np-Au can be viewed as an average response to many different features. Importantly, despite the distributions, the displayed features on np-Au are still significantly different than those on a planar gold surface (conceptualized as an infinitely wide single ligament). The net effect is that astrocyte coverage (despite some fluctuations as shown in Figure 8) is lower than the coverage for planar gold across the different feature distributions. This study, along with others covered in the review article by Dalby et al.,[48] confirms that different cell types exhibit unique responses to varying ranges of nanofeature size. The insensitivity of the neural cell response to the nanostructure sizes studied here presents possible avenues for "tuning" the morphology for other processes, such as modifying drug release kinetics from the film[25] or tuning the electrical properties of np-Au films[29] without altering the cell response elicited by np-Au surface topography.

Surface effects have been shown to drive many cellular processes, including proliferation, division, migration, and adhesion. Studies involving topographical effects have typically involved a single cell-type (e.g., neurons or astrocytes), which makes it difficult to simultaneously compare the responses of key neural cells. Topographical effects can influence cell response through several means: organization and spacing of integrins (critical molecules that mediate cell adhesion) along the cell membrane,[48] altered cytoskeletal formation affecting cell adhesion, as well as intracellular signaling cascades that can lead to more quiescent or reactive cell phenotypes.[49] The effect of surface roughness on different cell types has shown that cell response is highly dependent on the degree of the feature size. For example, integrin clustering and cellular adhesion is significantly altered on nanoscale pits in the size range of 70−300 nm.[48] Overall, the critical "bioactive" dimensions seen in the literature are generally on the order of ∼50 to hundreds of nanometers, which is in agreement with the characteristic feature sizes of the np-Au films tested in this study. As the np-Au film is obtained from a sputter-deposited thin film alloy on a flat glass surface, there is no microscale roughness (see Figure S1 in the Supporting Information). AFM measurements of the surface roughness of the np-Au films yield a root-mean-square roughness of 8−27 nm, which is below the critical dimensions that exhibit nanotopography-guided apoptosis and reduced adhesion, at least for neurons.[50] This suggests that lateral geometry (as opposed to height) plays a more important role in dictating the cellular responses observed in this study.

High-magnification images of astrocytes grown on the np-Au surface suggest that the np-Au surface morphology inhibits the initial spreading of astrocytes across the material surface. As seen in Figure 9, visual inspection of astrocytes grown on the np-Au surface shows a cell diameter at in vitro day 1 that is reduced compared to that of pl-Au and that has fewer cellular extensions forming on np-Au at both in vitro days 7 and 12 compared to pl-Au (also observed for a murine astrocytic cell line by Seker et al.[31]). Accordingly, a possible explanation for the differential response of astrocytes and neurons to the underlying surface is related to their unique morphologies. The typical neuron morphology includes a large proportion of long thin processes (e.g., neurites), whereas a typical astrocyte has a

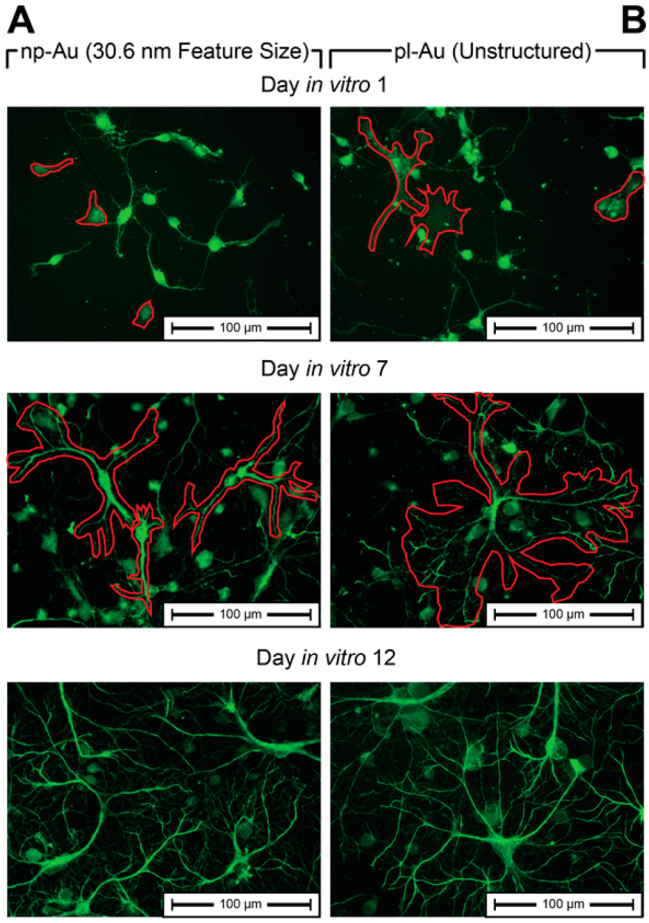

Figure 9. High magnification (40x) images of neurons and astrocytes at in vitro day 1, 7, and 12 on (A) standard np-Au and (B) unstructured pl-Au reveal cellular differences between astrocyte growth on np-Au and pl-Au. Astrocytes are highlighted by a red outline in the in vitro day 1 and 7 images. Because of the high nonspecificity of glial fibrillary acidic protein in perinatal neurons and astrocytes, neurons are also visible in the in vitro day 1 stains.[51] Astrocytes and neurons were differentiated visually through colocalization of tubulin-βIII and GFAP (not shown here).

higher ratio of thicker processes (Figure 1 and 9). The random topography provided by np-Au is permissive for thin cellular processes to align along a continuous path of ligaments and avoid the pores, which may constitute discontinuities that hinder cell spreading. In agreement with this hypothesis, on the planar gold surface, astrocytes exhibit a characteristic morphology, including long thick processes as seen in the SEM micrograph of a murine astrocyte (Figure S2 in the Supporting Information) acquired as described previously.[31] On the other hand, the np-Au surface limits astrocytic spreading to short and thin processes (Figure S3 in the Supporting Information) that align over continuous paths of ligaments (Figure S4 in the Supporting Information). Because epifluorescent images in Figure 1 indicate no difference in neuronal surface coverage on pl-Au or np-Au surfaces, it is reasonable to state that neurons with their typical morphology of long thin neurites are not affected by the underlying surface topographies studied here. In contrast, astrocytic coverage on pl-Au was clearly higher than on np-Au, as shown in Figure 1.

Ongoing experiments investigating focal adhesion formation, as well as gene expression changes in astrocytes on np-Au surfaces, should provide further insights into the dominant

DOI: 10.1021/acsami.5b00410
ACS Appl. Mater. Interfaces 2015, 7, 7093−7100

cellular mechanisms leading to the phenomena revealed in this paper.

4. CONCLUSIONS

In conclusion, we have shown that np-Au selectively reduces astrocytic coverage while maintaining high neuronal coverage in an in vitro neuron−glia co-culture model. More broadly, the study demonstrates a novel surface for supporting neuronal cultures without the use of culture medium supplements to reduce glial overgrowth.[52,53] A comprehensive analysis of the cytotoxic effects of residual silver in the np-Au films revealed that although residual silver can have an adverse effect on the viability of both neurons and astrocytes at high percentages, it is not the dominant cause for the observed selective reduction of the astrocytic surface coverage on np-Au films with <4 at. % silver. This was confirmed by conformally coating the surface of np-Au with aluminum oxide to mask any possible surface chemistry effects. Thus, topographical effects from the np-Au surface morphology have been validated as the dominant mechanism that leads to a noncytotoxic decrease in the ability of astrocytes to cover the np-Au surface. This passive reduction in astrocyte surface coverage demonstrates a nontoxic ability of np-Au to enhance the neuron-to-astrocyte surface coverage ratio in co-culture and may allow for improved neuron−electrode physical coupling. The surface morphology-driven decrease in astrocyte coverage presents a potential avenue for np-Au electrode coatings to provide additional mitigation of adverse tissue responses and enhancement of neuron−electrode coupling to np-Au-coated electrodes. Additionally, the ability of np-Au surface morphology to similarly affect astrocyte coverage in the regime from ∼30−100 nm enables tuning of the np-Au surface morphology for controlled release kinetics of small molecule drugs from the film.[25] This and other studies ongoing in our laboratory focus on studying histological and electrophysiological cortical cell response as a function of np-Au morphology to gain insight into the mechanisms by which morphology determines cortical cell coverage and recording fidelity. The differential effects of np-Au on astrocytic versus neuronal cell coverage reported in this study, coupled with previous demonstrations of high fidelity recordings from organotypic slices,[29] compatibility with microfabrication,[28] and reduction of astrocytic proliferation via in situ drug release from the np-Au patterns,[31] identify np-Au as a promising functional coating for chronic neural interfaces.

■ ASSOCIATED CONTENT

Supporting Information

Details of sample preparation, cell culture, surface functionalization, and imaging, as well as supporting scanning electron micrographs detailing the effect of nanotopography on cellular response. This material is available free of charge via the Internet at http://pubs.acs.org.

■ AUTHOR INFORMATION

Corresponding Author

*Address: 3177 Kemper Hall, Department of Electrical and Computer Engineering, University of California—Davis, Davis, CA 95616. E-mail: eseker@ucdavis.edu.

Notes

The authors declare no competing financial interest.

■ ACKNOWLEDGMENTS

We gratefully acknowledge support from UC Lab Fees Research Program Award [12-LR-237197], Research Investments in the Sciences & Engineering (RISE) Award, and UC Davis College of Engineering start-up funds. C.A.R.C. was supported by a National Science Foundation Graduate Research Fellowship [DGE-1148897] and a predoctoral fellowship from the National Institute of Health [T32-GM008799]. Support was also provided by the CounterACT Program, National Institutes of Health Office of the Director, and the National Institute of Neurological Disorders and Stroke [U54 NS079202]. H.C. was supported by a predoctoral fellowship from the National Institute of Environmental Health Sciences [T32 ES007059]; H.C. and M.S. received predoctoral fellowships from the Superfund Basic Research Program [P42 ES04699]. Any opinion, findings, and conclusions or recommendations expressed in this material are those of the authors(s) and do not necessarily reflect the views of the National Science Foundation or the National Institutes of Health. Work at LLNL was performed under the auspices of the U.S. DOE by LLNL [Contract DE-AC52-07NA27344].

■ REFERENCES

(1) Hochberg, L. R.; Serruya, M. D.; Friehs, G. M.; Mukand, J. A.; Saleh, M.; Caplan, A. H.; Branner, A.; Chen, D.; Penn, R. D.; Donoghue, J. P. Neuronal Ensemble Control of Prosthetic Devices by a Human with Tetraplegia. *Nature* **2006**, *442*, 164−171.

(2) Polikov, V. S.; Tresco, P. A.; Reichert, W. M. Response of Brain Tissue to Chronically Implanted Neural Electrodes. *J. Neurosci. Methods* **2005**, *148*, 1−18.

(3) Polikov, V. S.; Block, M. L.; Fellous, J.; Hong, J.; Reichert, W. M. In Vitro Model of Glial Scarring around Neuroelectrodes Chronically Implanted in the Cns. *Biomaterials* **2006**, *27*, 5368−5376.

(4) Woolley, A. J.; Desai, H. A.; Otto, K. J. Chronic Intracortical Microelectrode Arrays Induce Non-Uniform, Depth-Related Tissue Responses. *J. Neural Eng.* **2013**, *10*, 1−11.

(5) Ereifej, E. S.; Khan, S.; Newaz, G.; Zhang, J.; Auner, G. W.; VandeVord, P. J. Characterization of Astrocyte Reactivity and Gene Expression on Biomaterials for Neural Electrodes. *J. Biomed. Mater. Res., Part A* **2011**, *99*, 141−150.

(6) Fattahi, P.; Yang, G.; Kim, G.; Abidian, M. R. A Review of Organic and Inorganic Biomaterials for Neural Interfaces. *Adv. Mater.* **2014**, *26*, 1846−1885.

(7) Ilic, B.; Czaplewski, D.; Neuzil, P.; Stanczyk, T.; Blough, J.; Maclay, G. Preparation of Characterization of Platinum Black Electrodes. *Am. J. Mater. Sci. Technol.* **2000**, *35*, 3447−3457.

(8) Wessling, B.; Besmehn, A.; Mokwa, W.; Schnakenberg, U. Reactively Sputtered Iridium Oxide. *J. Electrochem. Soc.* **2007**, *154*, 83−89.

(9) Bruggemann, D.; Michael, K.; Wolfrum, B.; Offenhausser, A. Adhesion and Survival of Electrogenic Cells on Gold Nanopillar Array Electrodes. *Int. J. Nano Biomater.* **2012**, *4*, 108−127.

(10) Cui, X.; Hetke, J.; Wiler, J.; Anderson, D.; Martin, D. Electrochemical Deposition and Characterization of Conducting Polymer Polypyrrole/Pss on Multichannel Neural Probes. *Sens. Actuators* **2001**, *93*, 8−18.

(11) Wang, K.; Fishman, H.; Dai, H.; Harris, J. Neural Stimulation with a Carbon Nanotube Microelectrode Array. *Nano Lett.* **2006**, *6*, 2043−2048.

(12) Webster, T. J.; Waid, M. C.; McKenzie, J. L.; Price, R. L.; Ejiofor, J. U. Nano-Biotechnology: Carbon Nanofibres as Improved Neural and Orthopaedic Implants. *Nanotechnology* **2004**, *15*, 48−54.

(13) Kotov, N. A.; Winter, J. O.; Clements, I. P.; Jan, E.; Timko, B. P.; Campidelli, S.; Pathak, S.; Mazzatenta, A.; Lieber, C. M.; Prato, M.; Bellamkonda, R. V.; Silva, G. A.; Kam, N. W. S.; Patolsky, F.; Ballerini,

DOI: 10.1021/acsami.5b00410
ACS Appl. Mater. Interfaces 2015, 7, 7093−7100

L. Nanomaterials for Neural Interfaces. *Adv. Mater.* **2009**, *21*, 3970−4004.
(14) Spataro, L.; Dilgen, J.; Retterer, S.; Spence, A. J.; Isaacson, M.; Turner, J. N.; Shain, W. Dexamethasone Treatment Reduces Astroglia Responses to Inserted Neuroprosthetic Devices in Rat Neocortex. *Exp. Neurol.* **2005**, *194*, 289−300.
(15) Cui, X.; Wiler, J.; Dzaman, M.; Altschuler, R. A.; Martin, D. C. In Vivo Studies of Polypyrrole/Peptide Coated Neural Probes. *Biomaterials* **2003**, *24*, 777−787.
(16) Erlebacher, J.; Aziz, M.; Karma, A.; Dimitrov, N.; Sieradzki, K. Evolution of Nanoporosity in Dealloying. *Nature* **2001**, *410*, 450−453.
(17) Seker, E.; Reed, M. L.; Begley, M. R. Nanoporous Gold: Fabrication, Characterization, and Applications. *Materials* **2009**, *2*, 2188−2215.
(18) Santos, G. M.; Zhao, F.; Zeng, J.; Shih, W.-C. Characterization of Nanoporous Gold Disks for Photothermal Light Harvesting and Light-Gated Molecular Release. *Nanoscale* **2014**, *6*, 5718−5724.
(19) Li, K.; Huang, J.; Shi, G.; Zhang, W.; Jin, L. A Sensitive Nanoporous Gold-Based Electrochemical DNA Biosensor for *Escherichia coli* Detection. *Anal. Lett.* **2011**, *44*, 2559−2570.
(20) Feng, J.; Zhao, W.; Wu, J. A Label-Free Optical Sensor Based on Nanoporous Gold Arrays for the Detection of Oligodeoxynucleotides. *Biosens. Bioelectron.* **2011**, *30*, 21−27.
(21) Jin, H.-J.; Weissmüller, J. A Material with Electrically Tunable Strength and Flow Stress. *Science* **2011**, *332*, 1179−1182.
(22) Fujita, T.; Guan, P.; McKenna, K.; Lang, X.; Hirata, A.; Zhang, L.; Tokunaga, T.; Arai, S.; Yamamoto, Y.; Tanaka, N.; Ishikawa, Y.; Asao, N.; Yamamoto, Y.; Erlebacher, J.; Chen, M. Atomic Origins of the High Catalytic Activity of Nanoporous Gold. *Nat. Mater.* **2012**, *11*, 775−780.
(23) Hodge, A. M.; Hayes, J. R.; Caro, J. A.; Biener, J.; Hamza, A. V. Characterization and Mechanical Behavior of Nanoporous Gold. *Adv. Eng. Mater.* **2006**, *8*, 853−857.
(24) Lee, D.; Wei, X.; Chen, X.; Zhao, M.; Jun, S. C.; Hone, J.; Herbert, E. G.; Oliver, W. C.; Kysar, J. W. Microfabrication and Mechanical Properties of Nanoporous Gold at the Nanoscale. *Scr. Mater.* **2007**, *56*, 437−440.
(25) Kurtulus, O.; Daggumati, P.; Seker, E. Molecular Release from Patterned Nanoporous Gold Thin Films. *Nanoscale* **2014**, *6*, 7062−7071.
(26) Schade, L.; Franzka, S.; Mathieu, M.; Biener, M. M.; Biener, J.; Hartmann, N. Photothermal Laser Microsintering of Nanoporous Gold. *Langmuir* **2014**, *30*, 7190−7197.
(27) Bain, C. D.; Troughton, E. B.; Tao, Y. T.; Evall, J.; Whitesides, G. M.; Nuzzo, R. G. Formation of Monolayer Films by the Spontaneous Assembly of Organic Thiols from Solution onto Gold. *J. Am. Chem. Soc.* **1989**, *111*, 321−335.
(28) Daggumati, P.; Kurtulus, O.; Chapman, C. A. R.; Dimlioglu, D.; Seker, E. Microfabrication of Nanoporous Gold Patterns for Cell-Material Interaction Studies. *J. Visualized Exp.* **2013**, e50678.
(29) Seker, E.; Berdichevsky, Y.; Begley, M. R.; Reed, M. L.; Staley, K. J.; Yarmush, M. L. The Fabrication of Low-Impedance Nanoporous Gold Multiple-Electrode Arrays for Neural Electrophysiology Studies. *Nanotechnology* **2010**, *21*, 1−7.
(30) Tan, Y. H.; Terrill, S. E.; Paranjape, G. S.; Stine, K. J.; Nichols, M. R. The Influence of Gold Surface Texture on Microglia Morphology and Activation. *Biomater. Sci.* **2014**, *2*, 110−120.
(31) Seker, E.; Berdichevsky, Y.; Staley, K. J.; Yarmush, M. L. Microfabrication-Compatible Nanoporous Gold Foams as Biomaterials for Drug Delivery. *Adv. Healthcare Mater.* **2012**, *1*, 172−176.
(32) Gittard, S.; Pierson, B.; Ha, C.; Wu, C.; Narayan, R.; Robinson, D. Supercapacitive Transport of Pharmacologic Agents Using Nanoporous Gold Electrodes. *Biotechnol. J.* **2010**, *5*, 192−200.
(33) Patel, J.; Radhakrishnan, L.; Zhao, B.; Uppalapati, B.; Daniels, R. C.; Ward, K. R.; Collinson, M. M. Electrochemical Properties of Nanostructured Porous Gold Electrodes in Biofouling Solutions. *Anal. Chem.* **2013**, *85*, 11610−11618.
(34) Wayman, G. A.; Impey, S.; Marks, D.; Saneyoshi, T.; Grant, W. F.; Derkach, V.; Soderling, T. R. Activity-Dependent Dendritic Arborization Mediated by Cam-Kinase I Activation and Enhanced Creb-Dependent Transcription of Wnt-2. *Neuron* **2006**, *50*, 897−909.
(35) Erlebacher, J.; Aziz, M. J.; Karma, A.; Dimitrov, N.; Sieradzki, K. Evolution of Nanoporosity in Dealloying. *Nature* **2001**, *410*, 450−453.
(36) Biener, M. M.; Biener, J.; Wichmann, A.; Wittstock, A.; Baumann, T.; Baumer, M.; Hamza, A. ALD Functionalized Nanoporous Gold: Thermal Stability, Mechanical Properties, and Catalytic Activity. *Nano Lett.* **2011**, *11*, 3085−3090.
(37) George, S. M. Atomic Layer Deposition: An Overview. *Chem. Rev.* **2010**, *110*, 111−131.
(38) Howard, A. S.; Fitzpatrick, R.; Pessah, I.; Kostyniak, P.; Lein, P. J. Polychlorinated Biphenyls Induce Caspase-Dependent Cell Death in Cultured Embryonic Rat Hippocampal but Not Cortical Neurons Via Activation of the Ryanodine Receptor. *Toxicol. Appl. Pharmacol.* **2003**, *190*, 72−86.
(39) Arends, M. J.; Morris, R. G.; Wyllie, A. H. Apoptosis. The Role of the Endonuclease. *Am. J. Pathol.* **1990**, *136*, 593−608.
(40) Lonze, B. E.; Riccio, A.; Cohen, S.; Ginty, D. D. Apoptosis, Axonal Growth Defects, and Degeneration of Peripheral Neurons in Mice Lacking Creb. *Neuron* **2002**, *34*, 371−385.
(41) Zalups, R. K., Koropatnick, J., Eds. *Molecular Biology and Toxicology of Metals*; Taylor & Francis Inc: New York, 2000; Vol. *1*, p 609.
(42) Squire, L. R., Berg, D., Bloom, F. E., du Lac, S., Ghosh, A., Spitzer, N. C. *Fundamental Neuroscience*; Academic Press, 2008; Vol. *4*.
(43) Huang, C. L.; Hsiao, I. L.; Lin, H. C.; Wang, C. F.; Huang, Y. J.; Chuang, C. Y. Silver Nanoparticles Affect on Gene Expression of Inflammatory and Neurodegenerative Responses in Mouse Brain Neural Cells. *Environ. Res.* **2015**, *136*, 253−263.
(44) Bruggemann, D. Nanoporous Aluminium Oxide Membranes as Cell Interfaces. *J. Nanomater.* **2013**, *2013*, 460870-1−460870-18.
(45) Boutin, P.; Christel, P.; Dorlot, J. M.; Meunier, A.; de Requancourt, A.; Blanquaert, D.; Herman, S.; Sedel, L.; Witvoet, J. The Use of Dense Alumina-Alumina Ceramic Combination in Total Hip Replacement. *J. Biomed. Mater. Res.* **1988**, *22*, 1203−1232.
(46) Ludwig, K. A.; Uram, J. D.; Yang, J.; Martin, D. C.; Kipke, D. R. Chronic Neural Recordings Using Silicon Microelectrode Arrays Electrochemically Deposited with a Poly(3,4-ethylenedioxythiophene) (PEDOT) Film. *J. Neural Eng.* **2006**, *3*, 59−70.
(47) Spira, M. E.; Aviad, H. Multi-Electrode Array Technologies for Neuroscience and Cardiology. *Nat. Nanotechnol.* **2013**, *8*, 83−94.
(48) Biggs, M. J. P.; Richards, R. G.; Dalby, M. J. Nanotopographical Modification: A Regulator of Cellular Function through Focal Adhesions. *Nanomedicine* **2010**, *6*, 619−633.
(49) Morgan, J. T.; Murphy, C. J.; Russell, P. What Do Mechanotransduction, Hippo, Wnt, and Tgfb Have in Common? Yap and Taz as Key Orchestrating Molecules in Ocular Health and Disease. *Exp. Eye Res.* **2013**, *115*, 1−12.
(50) Brunetti, V.; Maiorano, G.; Rizzello, L.; Sorce, B.; Sabella, S.; Cingolani, R.; Pompa, P. P. Neurons Sense Nanoscale Roughness with Nanometer Sensitivity. *Proc. Natl. Acad. Sci. U.S.A.* **2010**, *107*, 6264−6269.
(51) Garcia, A. D. R.; Doan, N. B.; Imura, T.; Bush, T. G.; Sofroniew, M. V. GFAP-Expressing Progenitors Are the Principal Source of Constitutive Neurogenesis in Adult Mouse Forebrain. *Nat. Neurosci.* **2004**, *7*, 1233−1241.
(52) Billingsley, M. L.; Mandel, H. G. Effects of DNA Synthesis Inhibitors on Post-Traumatic Glial Cell Proliferation. *J. Pharmacol. Exp. Ther.* **1982**, *222*, 765−770.
(53) Dyhrfjeld-Johnsen, J.; Berdichevsky, Y.; Swiercz, W.; Sabolek, H.; Staley, K. Interictal Spikes Precede Ictal Discharges in an Organotypic Hippocampal Slice Culture Model of Epileptogenesis. *J. Clin. Neurophysiol.* **2010**, *27*, 418−424.

DOI: 10.1021/acsami.5b00410
ACS Appl. Mater. Interfaces 2015, 7, 7093−7100